Annals of Nuclear Energy 161 (2021) 108488

Contents lists available at ScienceDirect

Annals of Nuclear Energy

journal homepage: www.elsevier.com/locate/anucene

Review

Flow-induced vibration of tube bundles considering the effect of periodic fluid force in a rotated triangular tube array

Jiang Lai [a,*], Tiancai Tan [a], Shihao Yang [a], Lingling Lu [b], Lei Sun [a], Hongliang Ming [c]

[a] Nuclear Power Institute of China, Chengdu 610213, China
[b] Key Laboratory for Mechanics in Fluid Solid Coupling Systems, Institute of Mechanics, Chinese Academy of Sciences, Beijing 100190, China
[c] CAS Key Laboratory of Nuclear Materials and Safety Assessment, Institute of Metal Research, Chinese Academy of Sciences, Shenyang 110016, China

ARTICLE INFO

Article history:
Received 25 February 2021
Received in revised form 18 April 2021
Accepted 8 June 2021
Available online 22 June 2021

Keywords:
Flow-induced vibration
Tube bundles
Periodic fluid force
Vibration response

ABSTRACT

This paper investigated the flow-induced vibration of the tube bundles considering the effect of periodic fluid force in a rotated triangular tube array. We first performed an experiment to obtain the vibration responses of a rotated triangular tube array with the pitch-to-diameter ratio P/D = 1.48. To further investigate the vibration characteristics of the tube bundles, a mathematical model of the tube bundles considering the effect of the periodic fluid force and the clearance restriction was developed. Based on the Computational Fluid Dynamics calculation, the fluid force coefficients and the Strouhal numbers of the periodic fluid force in the tube bundles were determined. Considering the effect of the periodic fluid force, the vibration responses of the tube bundles were calculated. The vibration characteristics of the tube bundles induced by the periodic fluid force were discussed. The results demonstrated that some complex vibrations such as the beat vibrations and resonance may be induced by the periodic fluid force in the rotated triangular tube array, and the frequency of the periodic fluid force has a significant influence on the vibration characteristics of the tube bundles before the fluidelastic instability.

Contents

1. Introduction

Flow-induced vibration is a major concern in the design of nuclear steam generators. Due to the fretting wear between the tube bundles and support structures, some tube failures may occur leading to a nuclear accident. Thus, a great deal of research has been conducted. A number of papers have summarized that the flow excitation mechanisms can be classified as (a) turbulence, (b) vortex shedding, and (c) fluidelastic instability.

Turbulence-induced vibration has been analyzed by several scholars. Taylor et al. (Taylor et al., 1989) performed an extensive experiment to discuss the turbulence-induced vibration of the tube bundles subjected to two-phase cross-flow. Based on the experimental results, a normalized forced-excitation spectrum was formed as a design guideline of steam generators. Axisa et al.

* Corresponding author.
E-mail address: laijiang1983@163.com (J. Lai).

https://doi.org/10.1016/j.anucene.2021.108488
0306-4549/

carried out several experiments to investigate the turbulent buffeting of the tube arrays subjected to two-phase cross-flow. They found that in the high void fraction conditions, the random force of the air–water and steam-water would be of the same order of magnitude (Axisa et al., 1990). Langre et al. (Langre and Villard, 1998) proposed an upper bound on random buffeting forces caused by two-phase cross-flow in the tube bundles with the help of an experimental database. Taylor and Pettigrew (Taylor and Pettigrew, 2000) measured the fluid forces acting on the tube bundles in their experiments. The experimental results were used to determine the guidelines for random excitation forces. At the design stage of a steam generator, these guidelines can be used to estimate the turbulence-induced vibration of the tube bundles.

Fluidelastic instability is the excitation mechanism which may cause a short term failure of the steam generator tubes (Paidoussis, xxxx). With this potential for short term damage, many studies have been performed to investigate the fluidelastic instability of the tube bundles subjected to cross-flow. Price and Paidoussis (Price and Paidoussis, 1986) proposed a method to study the stability of a double row of flexible tubes subject to cross-flow. Lever and Weaver (Lever and Weaver, 1986a, 1986b) present a theoretical model to investigate the cross-flow induced fluidelastic instability in heat exchanger tube bundles. Nakamura et al. (Nakamura et al., 1992) carried out several experiments to investigate the fluidelastic vibration of the tube bundles both by air–water and steam-water flow. And, a new criterion, compared with the usual Connors-type criteria, was presented to estimate the fluidelastic instability. Austermann and Popp (Austermann and Popp, 1995) investigated the vibration behavior of the tube bundles subjected to air cross-flow. Their experimental results indicate that the array pattern has a significant influence on the threshold of the fluidelastic instability. Janzen et al. (Janzen et al., 2005) studied the vibration response of U-tubes in two-phase cross-flow in their experiments. The fluidelastic instability of the U-tubes in the transverse direction and the parallel direction was observed in the experiment. Hassan et al. (Hassan and Hayder, 2008) developed a time-domain model for fluidelastic instability forces of tubes with loose supports. The model can be used to calculate the critical flow velocity, tube response, and impact force between the tube and support. Chu et al. (Chu et al., 2009) experimentally investigated the fluidelastic instability of a U-tube array with pitch-to-diameter ratio P/D = 1.633 in two-phase cross-flow. The vibration responses of the U-tube bundles were measured to determine the instability constant of the Connors equation. Their experimental results show that, for the rotated square array with a pitch-to-diameter ratio P/D = 1.633, the fluidelastic instability constant is 8.5. Based on the linear lumped-parameter models, Harran (Harran, 2014) analyzed the influence of the mass ratio on the fluidelastic instability of the tubes in the transverse direction. Hassan and Mohany (Hassan and Mohany, 2016) present simulations of a loosely supported multi-span U-bend tube subjected to turbulence and fluidelastic instability forces. Borsoi et al. (Borsoi et al., 2017) investigated the turbulence-induced vibration and fluidelastic instability of a loosely supported tube, separately. Shinde et al. (Shinde et al., 2018) presented a theoretical model based on transient interactions between a single tube and the adjacent flow streams to study the fluidelastic instability of the tube bundles. Using this theoretical model, the critical velocity of the fluidelastic instability was obtained. Palomar and Meskell (Palomar and Meskell, 2018) calculated the static fluid force coefficient from steady RANS simulation. The pressure on the tube surface obtained from the calculational fluid dynamic (CFD) was compared with the experimental results to verify the correctness of the CFD methodology. Based on the numerical results, they found that the pitch ratio has the most effect on the threshold of the fluidelastic instability. Elhelaly et al. (Elhelaly et al., 2020) investigate the dynamics of loosely supported tube array subjected to cross-flow considering the effect of the flow approach angle and the clearance between the tube and the support.

Recently, we have performed a series of experimental studies to investigate the flow-induced vibration of a rotated triangular tube array subjected to two-phase cross-flow (Lai et al., 2019, 2020a, 2020b). The theoretical models to predict the critical velocity of the fluidelastic instability of the tube bundles have also been presented (Lai et al., 2019) (Lai, 2019). Based on these models, the nonlinear dynamic models of the tube bundles subjected to two-phase flow and loose support have been developed, and the two-phase flow-induced instability and nonlinear dynamic of the tube bundles have been investigated (Lai et al., 2019, 2020c, 2020d). These studies provide us with the theory for investigating the fluidelastic instability and the post-instability of the tube bundles.

As mentioned above, most experimental and numerical studies were carried out to investigate the fluidelastic instability associated with high flow pitch velocity in the tube bundles. It is important to note that, before the onset of the fluidelastic instability, some complex vibrations of the tube bundles were observed in the experiments (Taylor et al., 1989; Chung and Chu, 2006), which were different from the vibration characteristics of the turbulence-induced vibration. Some scholars speculated that the vortex shedding vibration of the tube bundles occurred. However, there are few specific verifications and quantitative studies given.

In this study, experimental and theoretical analyses were conducted to investigate the vibration characteristics of the tube bundles subjected to cross-flow. First, the experimental measurements of the vibration responses of the tube bundles in the transverse direction were carried out. Then, a mathematical model of the flow-induced vibration of the tube bundles considering the effect of the periodic fluid force was established. To obtain the fluid force coefficient and the frequency of the periodic fluid force in a rotated triangular tube array with the pitch-to-diameter ratio P/D = 1.48, a calculation of the Computational Fluid Dynamics was presented. Last, considering the effect of the periodic fluid force, the vibration responses of the tube bundles were calculated. The vibration characteristics of the tube bundles induced by the periodic fluid force were discussed.

2. Experimental analysis

The measurements of the vibration response of the tube bundles subjected to cross-flow were conducted using the experimental loop shown in Fig. 1. It includes two loops, one is a water loop and another is an air loop. In this experiment, only the water loop was used. The max rated flow of the water loop is 1200 m^3/h, the max operating pressure is 1.6 MPa, and the max operating temperature is 80 ℃. Magnetic flowmeter was used to measure the water flow rate. A more comprehensive description of this experimental loop was presented in reference (Lai et al., 2019). All measurements were conducted at room temperature (approximately 20 ℃).

The experimental test section is shown in Fig. 2. The tube array in the test section is a rotated triangular tube array composed of seven columns of tubes and two columns of half-tube attached to the walls, all arranged in fifteen rows, as shown in Fig. 3. The tube diameter is 0.01745 m, the tube length is 0.312 m, and the pitch-to-diameter ratio is 1.48. The tube bundles were fixed in the test section. All the tubes were supported with a flexible cantilever beam, called the frequency control unit, to limit to move in the transverse direction. The fundamental natural frequency of the tube bundles in air is 40 Hz in the transverse direction and 80 Hz in the parallel direction, respectively. The strain gauges were mounted on the flexible beam near the clamped end to measure the strains of the tube bundles at the transverse direction.

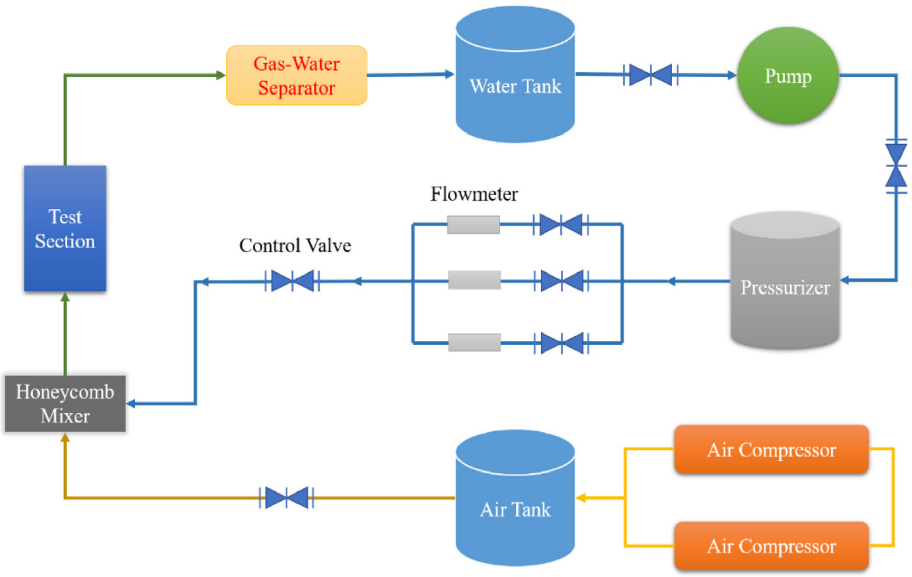

Fig. 1. Schematic diagram of the two-phase test loop.

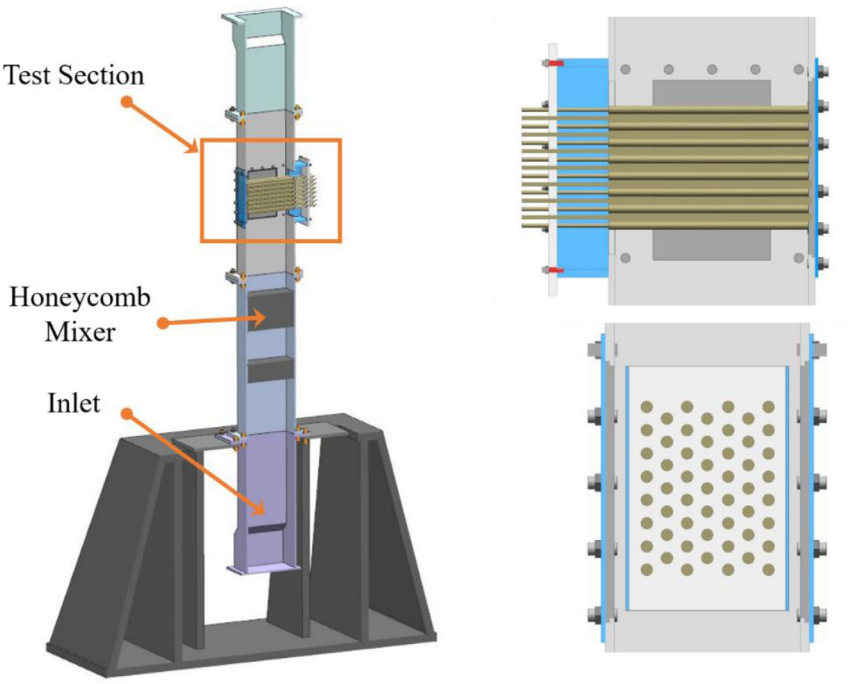

Fig. 2. Schematic diagram of the experiment model.

The vibration response tests were conducted for various flow pitch velocities. In the experiment, the flow pitch velocity was increased progressively and the strains of five tubes (tube 1, tube 2, tube 3, tube 4, and tube 5, as shown in Fig. 3) were measured. The root-mean-square (RMS) strains of the five tubes were illustrated in Fig. 4. When the flow pitch velocity is less than 0.7 m/s, the turbulence-induced vibration of the tube bundles can be observed for all five tubes. The increasing rate of the RMS strains of the tube bundles with the flow pitch velocity is not significant. When the flow pitch velocity is higher than 0.7 m/s, with the increasing of the flow pitch velocity, the RMS strains of the tube bundles increases gradually. When the flow pitch velocity is above 1.28 m/s, the RMS strains of the tube bundles show a sharp increase with respect to a small increase in the flow pitch velocity, which can be defined as the threshold of the fluidelastic instability. As we know, the fluidelastic instability is a typical self-excited vibration, when the fluidelastic instability occurs, a periodic oscillation of the tubes can be observed. However, in the present experiment, it is interesting to note that before the fluidelastic instability, the tube bundles vibrations with large amplitude and two frequencies can be observed which are different from the vibration characteristics of the fluidelastic instability. The vibration response time histories of the five tubes when the flow pitch velocity is 1.2 m/s were shown in Fig. 5, which are "beat" signals. It is important to note that the beat vibration is a forced oscillation induced by a periodic force when the force frequency closes to

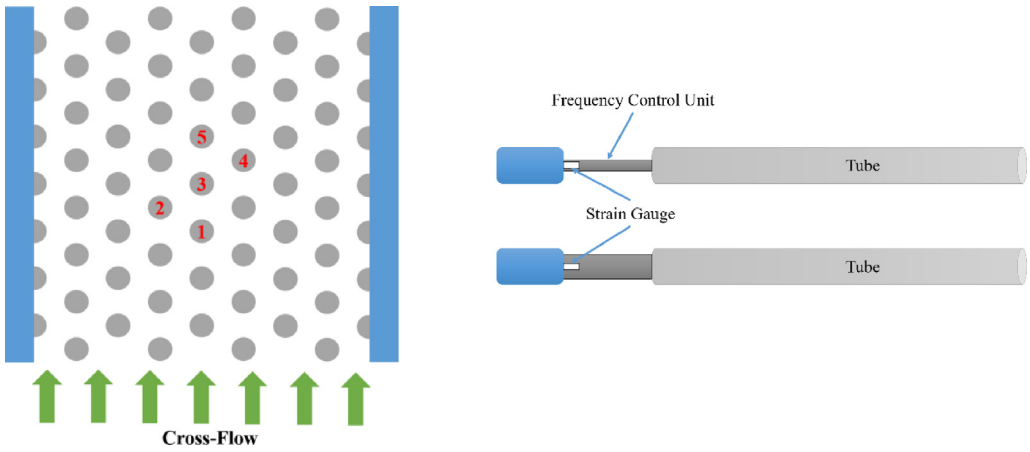

Fig. 3. Schematic diagram of a rotated triangular tube array.

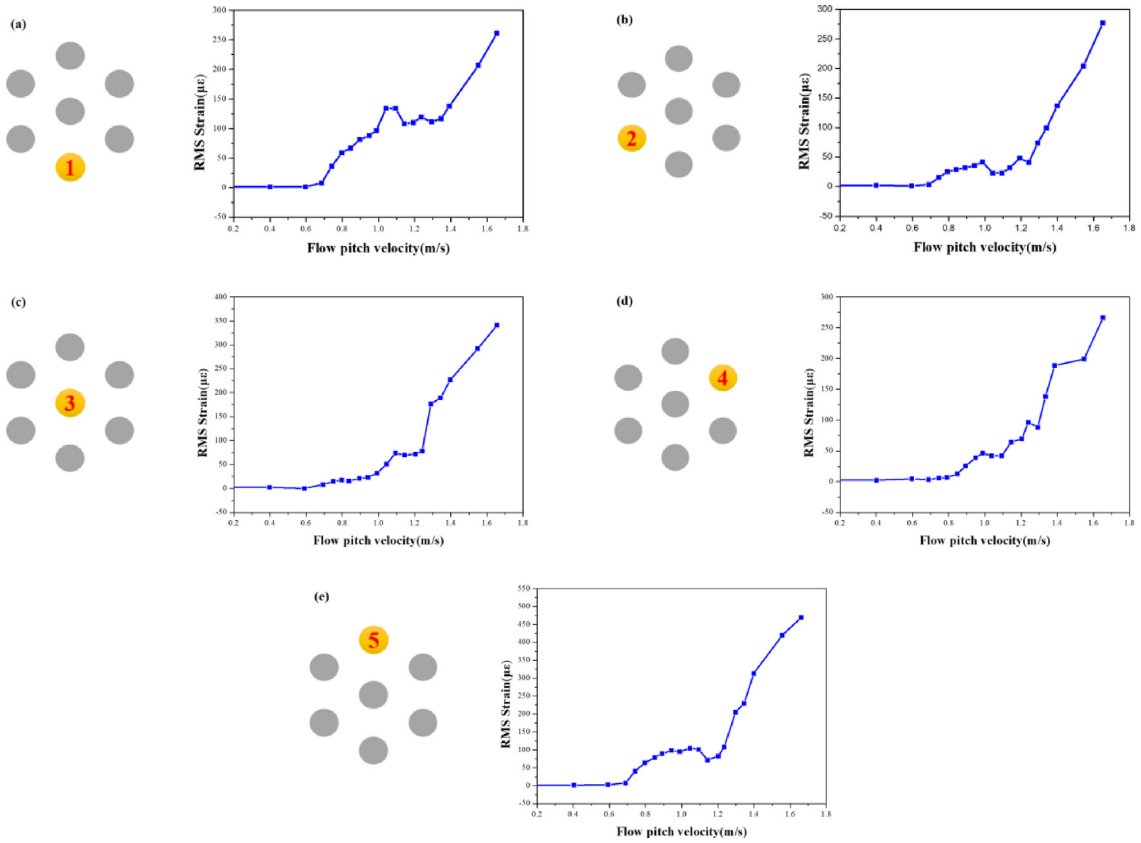

Fig. 4. RMS strain amplitude of the five tubes in the transverse direction versus flow pitch velocity: (a) tube 1; (b) tube 2; (c) tube 3; (d) tube 4; (e) tube 5.

the natural frequency of the tube. And, the vibration amplitudes of the upstream tubes are larger than those of the downstream tubes.

The vibration frequency spectra of the five tubes when the flow pitch velocity is 1.2 m/s were illustrated in Fig. 6. It is clearly seen that there are three main frequencies (f_1 = 29.0 Hz, f_2 = 30.4 Hz, f_3 = 31.9 Hz). f_1 is the system frequency of the experimental apparatus resulting from the pump. According to our previous study (Lai et al., 2019), it is known that f_3 is the fundamental natural frequency of the tube in water. Thus, it is reasonable to believe that f_2 is the frequency of the force which causes the beat vibration of the tube bundles. To verify the correctness of this speculation, the theoretical and numerical analyses were carried out in the next sections.

3. Theoretical analysis

It is known that, in a steam generator, the tube bundles are threaded through support structures, such as the tube support plate (TSP) and anti-vibration bars (AVBs). There is certain expansion clearance between the tube bundles and support structures which can prevent deformation of the heated surface due to restrained expansion. When the flow pitch velocity is low, there won't be any collision between the tube bundles and support structures. Once the flow pitch velocity is larger than the threshold of the fluidelastic instability, the collision may take place. The tube support plate and anti-vibration bars may change the support stiffness of the tube bundles system, leading to a change in the vibra-

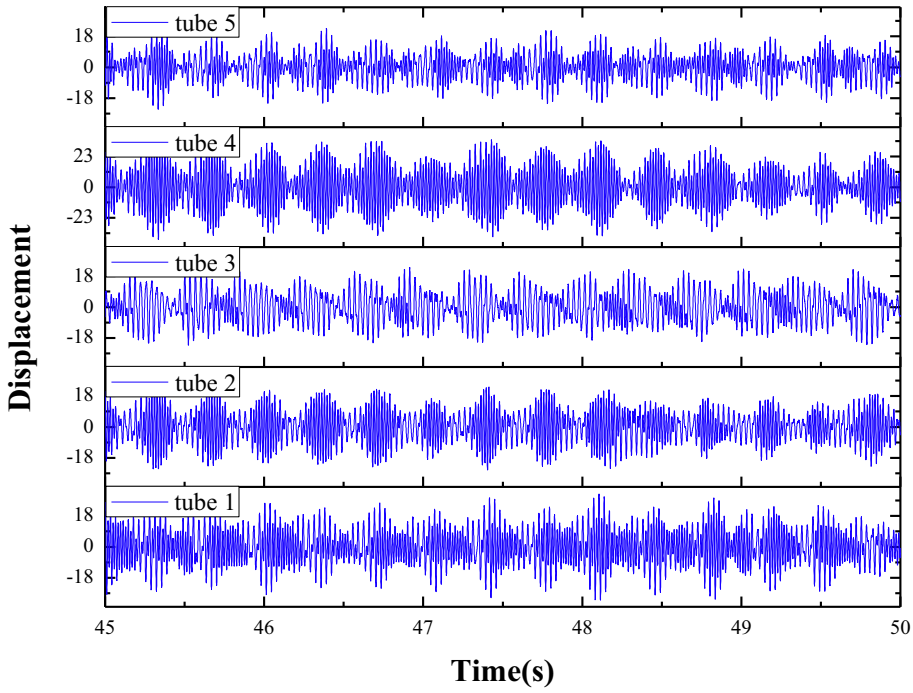

Fig. 5. The vibration response time histories of the five tubes in the transverse direction at U_p = 1.2 m/s.

tion frequency of the tube bundles, once the fluidelastic instability occurs. In other words, before the onset of fluidelastic instability, the vibration amplitude of the tube is less than the gap between the tube and the support. The support has little effect on the vibration response of the tube. Thus, considering the effect of the periodic fluid force and the support structures, the vibration equation of a flexible tube in tube bundles subjected to cross-flow and clearance restriction, as shown in Fig. 7, was presented as follows:

$$EI\frac{\partial^4 w}{\partial y^4}+c_t\frac{\partial w}{\partial t}+m_t\frac{\partial^2 w}{\partial t^2}+\delta(y-y_a)f(w) = F_{fluidelastic}(w,\dot{w},\ddot{w})+F_{periodic}(C_L,\quad \omega_S,\quad t) \tag{1}$$

where E is the elasticity modulus, I is the cross-sectional moment of inertia, c_t is the damping per length, m_t is the mass of the tube per length, $\delta(y\text{-}y_a)f(w)$ is the impact force between the tube bundles and the support structures, $F_{fluidelastic}(w,\dot{w},\ddot{w})$ is the steady fluid force, $F_{periodic}(C_L, \omega_S, t)$ is the periodic fluid force, C_L is the lift force coefficient, ω_S is the circular frequency of the periodic fluid force, φ is the phase angle.

The fluidelastic fluid force of the cross-flow acting on the tube can be written as:

$$F_{fluidelastic}(w,\dot{w},\ddot{w}) = m_a\frac{\partial^2 w(y,t)}{\partial t^2}+c_a\frac{\partial w(y,t)}{\partial t}+k_a w(y,t) \tag{2}$$

where m_a, c_a, and k_a is the added mass, added damping, and added stiffness, respectively, which can be expressed as:

$$\begin{aligned} m_a &= \tfrac{\pi}{4}\rho D^2\left[\tfrac{(D_e/D)^2+1}{(D_e/D)^2-1}\right] \\ c_a &= \tfrac{1}{2}\tfrac{\rho U_\infty^2 C_F\sin\Phi_F}{\omega} \\ k_a &= \tfrac{1}{2}\rho U_\infty^2 C_F\cos\Phi_F \end{aligned} \tag{3}$$

where ρ is the cross-flow density, U_∞ is the stream velocity, D is the tube diameter, ω is the angular fundamental frequency of the tube, C_F is the force coefficients, Φ_F is the fluid force phase (Sawadogo and Mureithi, 2014); D_e/D is a confinement parameter given as:

$$D_e/D = \left(0.96+0.5\frac{P}{D}\right)\frac{P}{D} \tag{4}$$

The flow pitch velocity of the tube bundles can be expressed as:

$$U_p = U_\infty\frac{P}{P-D} \tag{5}$$

The periodic fluid force of the cross-flow acting on the tube bundles can be expressed as:

$$F_{periodic}(t) = \frac{1}{2}\rho D U_\infty^2 C_L\sin(\omega_S t+\varphi) \tag{6}$$

Introducing the following the non-dimensional quantities:

$$\begin{aligned} &\eta=\frac{w}{D},\quad \xi=\frac{y}{L},\quad \tau=\lambda_1^2\sqrt{\frac{EI}{m_t L^4}}t=\Omega t,\quad \varsigma=\frac{c_t}{\Omega m_t},\quad m^*=\frac{m_t}{\rho D^2},\\ &U^*=\frac{2\pi U_\infty}{D\Omega},\alpha=\frac{1}{1+4m^*/(\pi C_{ma})},\quad \omega^*=\frac{\omega}{\Omega},\\ &\omega^{**}=\frac{\omega_S}{\Omega},C_L^*=DC_L \end{aligned} \tag{7}$$

where L is the tube length, λ_1 is the dimensionless eigenvalue of the first-order mode for a cantilever beam, C_{ma} is the added mass coefficient which can be expressed as (Pettigrew et al., 1989):

$$C_{ma} = \frac{(D_e/D)^2+1}{(D_e/D)^2-1} \tag{8}$$

By substituting these dimensionless quantities into equation (1), the partial differential equation of the motion of the tube bundles considering the effects of two-phase cross-flow and clearance restriction can be rewritten as:

$$\begin{aligned} &\tfrac{1}{1-\alpha}\tfrac{\partial^2\eta}{\partial\tau^2}(\xi,\tau)+\left[\varsigma-\tfrac{U^{*2}C_F\sin\Phi_F}{8\pi^2 m^*\omega^*}\right]\tfrac{\partial\eta}{\partial\tau}(\xi,\tau)+\tfrac{1}{\lambda_1^4}\tfrac{\partial^4\eta}{\partial\xi^4}(\xi,\tau)\\ &-\left[\tfrac{U^{*2}C_F\cos\Phi_F}{8\pi^2 m^*}-\tfrac{\alpha\omega^{*2}}{1-\alpha}\right]\eta(\xi,\tau)+\delta(\xi-\xi_b)f^*(\eta)=\tfrac{U^{*2s}}{8\pi^2 m^*}C_L^*\sin(\omega^{**}\tau) \end{aligned} \tag{9}$$

According to the Galerkin method, it is reasonable to suppose that:

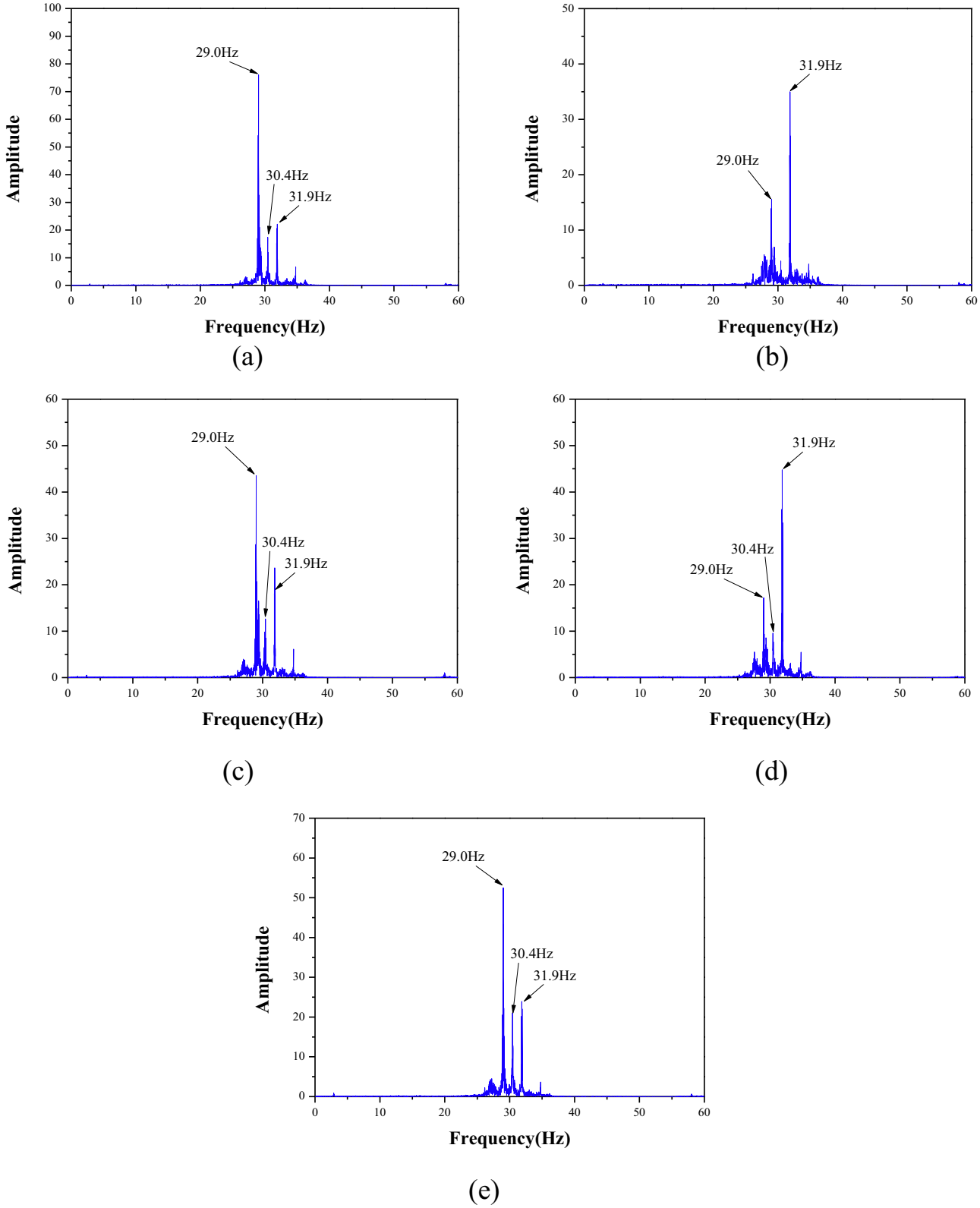

Fig. 6. The frequency spectrum of the tube bundles at U_p = 1.20 m/s: (a) tube 1; (b) tube 2; (c) tube 3; (d) tube 4; (e) tube 5.

$$\eta(\xi,\tau)=\sum_{i=1}^{N}\varphi_i(\xi)q_i(\tau) \tag{10}$$

where $\varphi_i(\xi)$ is the modal shape of the simply supported tube. It is known that the dynamic response of a tube is dominated by the first low modes. Thus, the first five order modes (N = 5) were chosen in the present study.

Using the Galerkin expansion and modal truncation techniques, a set of ordinary differential equations can be deduced from the partial differential equation, as follows:

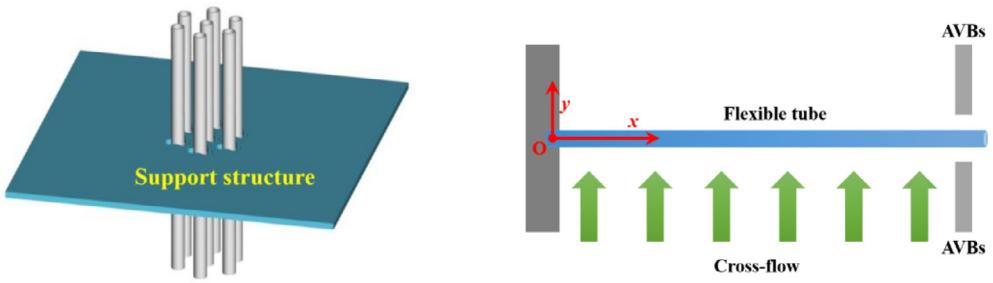

Fig. 7. Schematic diagram of the tube bundles subjected to cross-flow and clearance restriction.

$$\frac{\ddot{q}_i}{1-\alpha}+\left(\zeta-\frac{U^{*2}C_F\sin\Phi_F}{8\pi^2 m^*\omega^*}\right)\dot{q}_i+\left(\frac{\lambda_i^4}{\lambda_1^4}-\frac{U^{*2}C_F\cos\Phi_F}{8\pi^2 m^*}+\frac{\alpha\omega^{*2}}{1-\alpha}\right)q_i+f^*(\eta_a)\varphi_i(\xi_a)=\frac{U^{*2}}{8\pi^2 m^*}C_L^*\sin(\omega^{**}\tau)(i=1,\quad 2,\quad 3,\quad 4,\quad 5) \tag{11}$$

where η_a is the displacement at $\xi = \xi_a$.

Notice that the coupling term is the impact force between the tube and tube support plate $f^*(\eta_a)$ due to the constraint at the clearance restriction. In this study, the mathematical model presented by Paidoussis et al. (Sawadogo and Mureithi, 2014) was used to represent properly the restraining force of clearance restriction, which can be written as:

$$f^*(\eta_a)=\kappa\left[\eta_a-\frac{1}{2}(|\eta_a+d|-|\eta_a-d|)\right]^3 \tag{12}$$

where d is the gap between the tubes and the support structures, κ is the non-dimensional stiffness of the clearance restriction. In this paper, κ is chosen to be 5.6×10^6 in accordance with reference (Paidoussis et al., 1991).

4. Numerical analysis

The last section provides the analysis method to study the fluid–structure interaction of the tube bundles subjected to cross-flow and clearance restriction. On the basis of the analyses above, the quantitative analysis was conducted. Firstly, according to the experimental model, a calculation of the Computational Fluid Dynamics (CFD) was presented to obtain the force of the periodic fluid force acting on the rotated triangular tube array with P/D = 1.48 in section 4.1. Then, considering the effect of the periodic fluid force, the vibration responses of the tube bundles before the onset of fluidelastic instability were calculated in section 4.2.

4.1. CFD calculation

To obtain the lift force coefficient and the circular frequency of the periodic fluid force acting on the tube bundles, a calculation of the Computational Fluid Dynamics was presented. Commercial CFD calculation programs ANSYS Fluent was utilized to solve the governing equations of continuity, momentum, energy, and turbulence quantities.

The standard k-ε model based on model transport equations for the turbulence kinetic energy, k, and its dissipation rate, ε, was used to calculate the cross-flow in a rotated triangular tube array. The turbulence kinetic energy, k, and its rate of dissipation, ε, can be obtained from the following transport equations:

$$\begin{aligned}\frac{\partial\rho k}{\partial t}+\frac{\partial\rho k u_i}{\partial x_i}&=\frac{\partial}{\partial x_j}\left[\left(\mu+\frac{\mu_t}{\sigma_k}\right)\frac{\partial k}{\partial x_j}\right]+G_k+G_b-\rho\varepsilon-Y_M\\ \frac{\partial\rho\varepsilon}{\partial t}+\frac{\partial\rho\varepsilon u_i}{\partial x_i}&=\frac{\partial}{\partial x_j}\left[\left(\mu+\frac{\mu_t}{\sigma_e}\right)\frac{\partial e}{\partial x_j}\right]+C_{1\varepsilon}\frac{\varepsilon}{k}(G_k+C_{3\varepsilon}G_b)-C_{2\varepsilon}\rho\frac{\varepsilon^2}{k}\end{aligned} \tag{13}$$

where G_k is the generation of turbulence kinetic energy due to the mean velocity gradients, G_b is the generation of turbulence kinetic energy due to buoyancy, Y_M represents the contribution of the fluctuating dilatation incompressible turbulence to the overall dissipation rate, $C_{1\varepsilon}$, $C_{2\varepsilon}$, and $C_{3\varepsilon}$ are constants, σ_k, and σ_ε are the turbulent Prandtl numbers for k and ε, respectively.

The turbulence viscosity, μ_t, can be written as:

$$\mu_t=\rho C_\mu\frac{k^2}{\varepsilon} \tag{14}$$

The values of the model constants $C_{1\varepsilon}$, $C_{2\varepsilon}$, C_μ, σ_k, and σ_ε, determined from experiments for fundamental flows including frequently encountered shear flows.

As shown in Fig. 8, according to the experimental model used in the last section, a 2-D flow domain was established to represent the tube bundles with the pitch-to-diameter ratio P/D = 1.48. the upstream and downstream length is 5.2D and 16.7D, respectively. A comprehensive description of the mesh sensitivity analysis of this model was conducted in our previous study (Lai et al., 2020e). The grid model used for flow field calculation in the present study was illustrated in Fig. 9.

The transient analysis of the periodic fluid force in a rotate triangular tube array was conducted with the flow pitch velocity ranging from 0.5 m/s to 1.5 m/s, and reasonable numerical results were obtained. An example of the lift force coefficient of the peri-

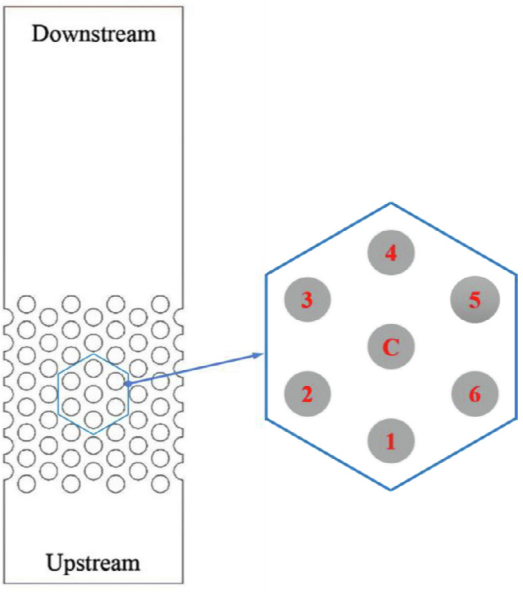

Fig. 8. Schematic diagram of the CFD model.

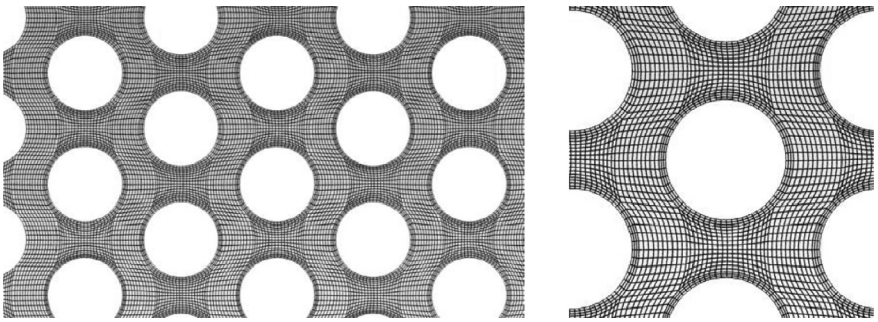

Fig. 9. Near-wall mesh inside the tube array.

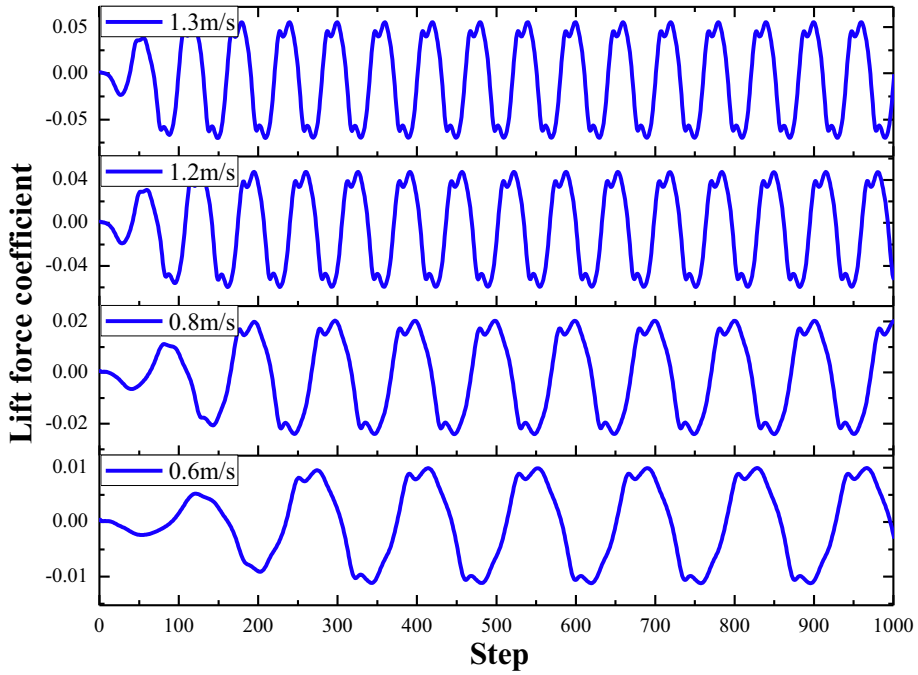

Fig. 10. The example of the time histories of the lift force coefficient of the central tube.

odic fluid force acting on the central tube for four flow pitch velocity conditions (U_p = 0.6 m/s, U_p = 0.8 m/s, U_p = 1.2 m/s, and U_p = 1.3 m/s) was illustrated in Fig. 10. The phenomenon of periodic fluid force can be obviously observed. It is important to note that the lift force coefficient and the frequency of the periodic fluid force increase with the increase of the flow pitch velocity. In order to more clearly illustrate the influence of the flow pitch velocity on the frequency of the periodic fluid force, the frequency spectrum of the lift force coefficients as shown in Fig. 11. It can be clearly seen that when the flow pitch velocity is low (e.g. U_p = 0.5 m/s, U_p = 0.6 m/s, and U_p = 0.8 m/s), the periodic fluctuation characteristics of the cross-flow is very weak which can be neglected. For the high flow pitch velocity conditions (e.g. U_p = 1.2 m/s, U_p = 1.3 m/s, and U_p = 1.5 m/s), the periodic fluctuation characteristics of the flow become highly obvious, and the frequency of the periodic fluid force has a significant variation with the increase of the flow pitch velocity. As shown in Fig. 11, when the flow pitch velocity is 1.2 m/s, the frequency of the periodic fluid force is 30.6 Hz. When the flow pitch velocity is 1.3 m/s, the frequency of the periodic fluid force is 33.2 Hz. When the flow pitch velocity is 1.5 m/s, the frequency of the periodic fluid force is 38.4 Hz.

For a better description of the periodic fluctuation characteristics of the flow, the Strouhal number of the periodic fluid force in the rotated triangular tube array was calculated. The Strouhal number, S_t, is an important dimensionless parameter to describe the periodic characteristics of the periodic fluid force, which can be expressed as:

$$S_t = \frac{fD}{U_p} = \frac{\omega_S D}{2\pi U_p} \tag{15}$$

The Strouhal numbers of the periodic fluid force for the six flow pitch velocity conditions considered in this study were illustrated in Fig. 12. The Strouhal number of the periodic fluid force in a rotated triangular tube array with P/D = 1.48 is about 0.42, and presents fewer variations when the Reynolds number ranging from 0.8×10^5 to 2.8×10^5. It is the main reason that with the flow pitch velocity ranging from 1.3 m/s to 1.5 m/s, the frequency of the periodic fluid force changes from 33.2 Hz to 38.4 Hz. Thus, we can confirm that in Fig. 6, besides the peak of the fundamental natural frequency of the tube in water, the other two peaks are the external exciting frequencies of the forces acting on the tube bundles. One is the system frequency of the experimental loop, the other is the frequency of the periodic fluid force in the tube array.

On the other hand, a comparison of the static pressure and turbulent intensity distribution between the six tubes was presented in Fig. 13. It can be clearly seen that the static pressure and turbulent intensity distributions of the upstream tubes are similar to those of the downstream tubes. The fluid forces acting on the

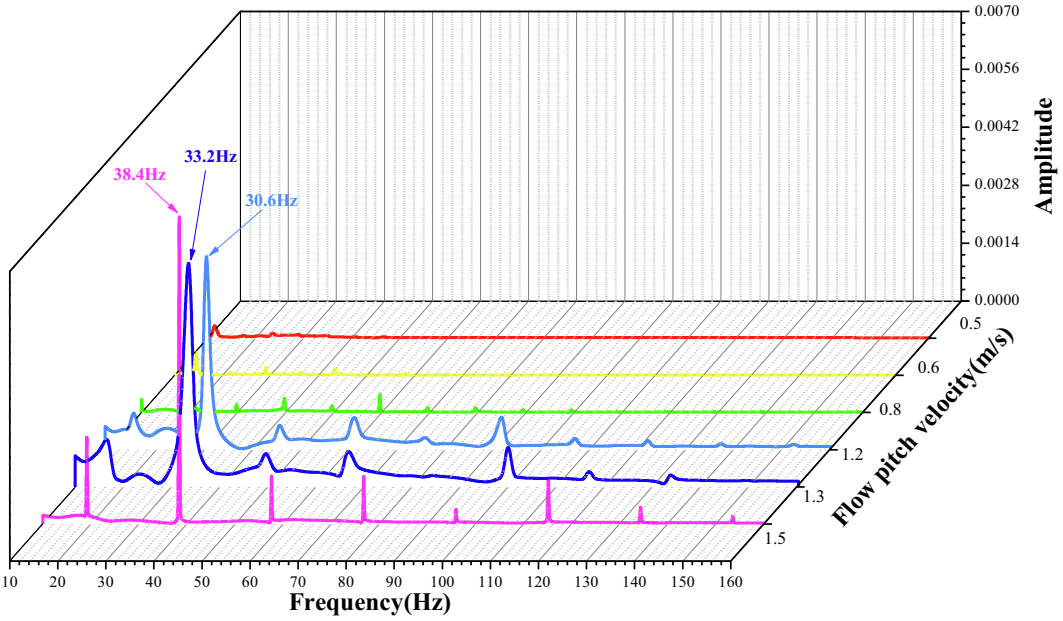

Fig. 11. Frequency spectrum of the lift force coefficient.

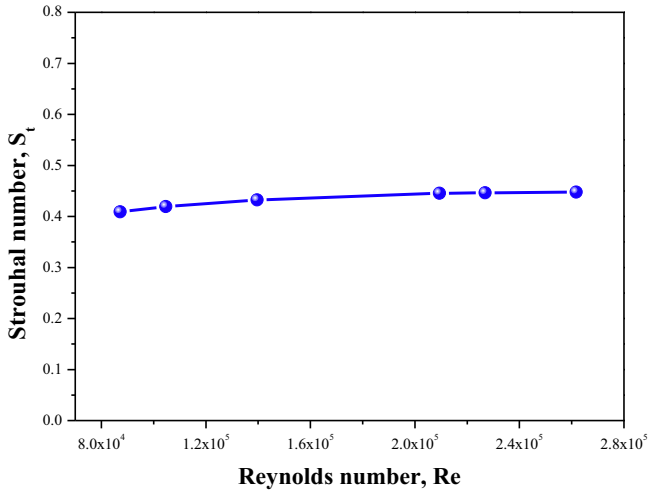

Fig. 12. Strouhal number of the periodic fluid force in tube bundles.

upstream tubes are larger than those acting on the downstream tubes. An obvious asymmetry of the static pressure and turbulent intensity distributions between tube 2 and tube 6, tube 3 and 5 can be observed.

4.2. Vibration response calculation

Fig. 14 is a supercritical bifurcation diagram for tube bundles considering the effect of cross-flow and the support structures. The flow pitch velocity at the Hopf bifurcation point is the critical velocity of the fluidelastic instability. When the flow pitch velocity is lower than the critical velocity, the tube bundles system is stable. Once the flow pitch velocity is larger than the threshold of the fluidelastic instability, the system may become unstable. The correct method for calculating the bifurcation diagram and the nonlinear dynamic characteristics of the tube bundles subjected to two-phase cross-flow and loose support have been investigated in our previous studies (Lai et al., 2019, 2020c, 2020d). Fig. 15.

When the flow pitch velocity is lower than the Hopf bifurcation velocity, the vibration amplitude of the tube is less than the gap between the tube and support structure, the tube bundles system can be treated as a linear vibrating system at the equilibrium position. The non-dimensional linearized equations at the equilibrium position can be written as:

$$\frac{\ddot{q}_i}{1-\alpha}+\left(\zeta-\frac{U^{*2}C_F\sin\Phi_F}{8\pi^2 m^*\omega^*}\right)\dot{q}_i + \left(\frac{\lambda_i^4}{\lambda_1^4}-\frac{U^{*2}C_F\cos\Phi_F}{8\pi^2 m^*}+\frac{\alpha\omega^{*2}}{1-\alpha}\right)q_i=0 \quad (i=1,\ 2,\ 3,\ 4,\ 5) \tag{16}$$

In the shorthand of matrix analysis, the generalized coordinates are expressed as:

$$\boldsymbol{Q}=[\dot{q}_1\ \ \dot{q}_2\ \ \dot{q}_3\ \ \dot{q}_4\ \ \dot{q}_5\ \ q_1\ \ q_2\ \ q_3\ \ q_4\ \ q_5]^T \tag{17}$$

The reduced-order equations can be expressed as:

$$\dot{\boldsymbol{Q}}=\boldsymbol{A}\boldsymbol{Q} \tag{18}$$

where ξ=(0, η_0) represents the equilibrium position, **A** is the Jacobian matrix, which can be expressed as:

$$\boldsymbol{A}=\begin{bmatrix}-\boldsymbol{M}^{-1}\boldsymbol{C} & -\boldsymbol{M}^{-1}\boldsymbol{K}\\ \boldsymbol{I} & \boldsymbol{O}\end{bmatrix} \tag{19}$$

where **M** is the mass matrix, **C** is the damping matrix, **K** is the stiffness matrix, **I** is the identity matrix, **O** is the zero matrix.

According to Lyapunov's indirect method, the stability of the nonlinear tube bundles system described by equation (11) in the neighborhood of its equilibrium point can be determined by the eigenvalues of Jacobian matrix **A**. A comprehensive description of the method to predict the critical velocity of the fluidelastic instability was presented in reference (Lai et al., 2019; Lai, 2019). Fig. 16 illustrates the real part of the eigenvalue corresponding to the fluidelastic instability mode of the tube. The flow pitch velocity corresponding to the zero-real part of the eigenvalue is the threshold of the fluidelastic instability of the tube bundles. For the example considered in this study, the fundamental frequency of the tube

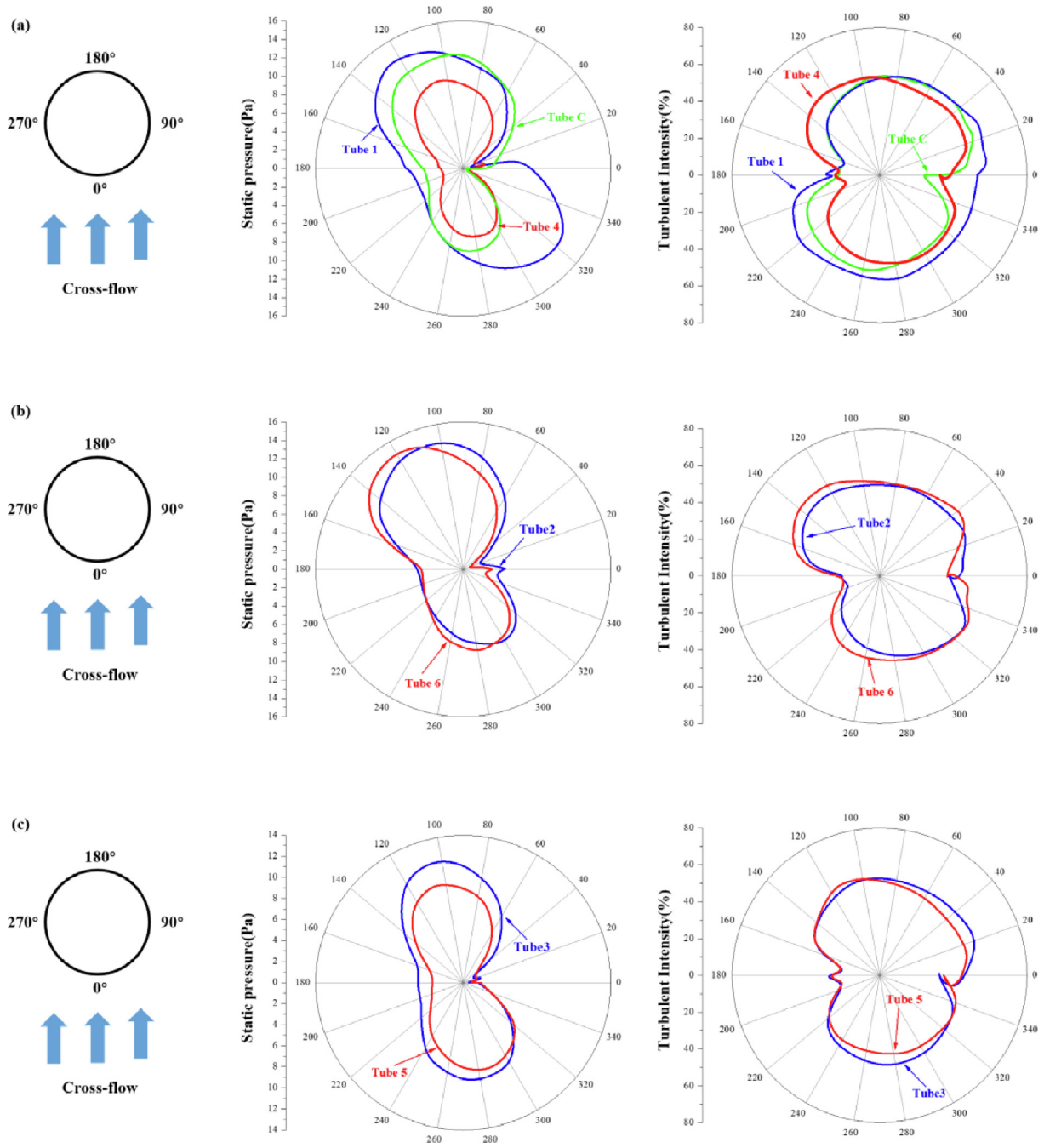

Fig. 13. Static pressure and turbulent intensity distributions for the six tubes at U_p = 1.2 m/s: (a) tube C, tube 1, and tube 4; (b) tube 2 and tube 6; (c) tube 3 and tube 5.

in the transverse direction is 40 Hz, the critical velocity of the fluidelastic instability is 1.28 m/s, which shows a satisfactory agreement with the experimental results in the last section.

To investigate the vibration characteristics of the tube bundles before the onsetof fluidelastic instability, a fourth-order variable step-size Runge-Kutta integration algorithm was used to calculate the dynamic responses of the tube bundles for the five flow pitch velocity conditions (U_p = 0.5 m/s, U_p = 0.6 m/s, U_p = 0.8 m/s, U_p = 1.2 m/s, and U_p = 1.3 m/s, respectively). Fig. 16 shows the vibration responses of the tube at $\xi = \xi_a$ for the first four cases (U_p = 0.5 m/s, U_p = 0.6 m/s, U_p = 0.8 m/s, and U_p = 1.2 m/s, respectively). According to the analysis above, it is known that the fluidelastic instability does not occur, the tube vibration is a forced oscillation induced caused by a periodic force. When the flow pitch velocity is lower than 0.7 m/s, the frequency of the periodic force is much less than the fundamental frequency of the tube in water, and the periodic excitation is very small. Therefore, it can be clearly seen that the amplitudes of the periodic vibration of the tube at U_p = 0.5 m/s and U_p = 0.6 m/s are relatively small. At U_p = 0.8 m/s, the amplitude of the vibration of the tube is obviously increased, and the multiple frequency vibration induced by the periodic fluid force can be observed. At U_p = 1.2 m/s, the frequency of the periodic fluid force is close to the tube fundamental frequency. According to the theory of vibrate dynamics, it is known that when the frequency of the force acting on the system is close to the fundamental natural frequency of the structure, a beat vibration may occur, which has been observed in the experiment. The amplitude of the beat vibration is much larger than those of the other cases. It

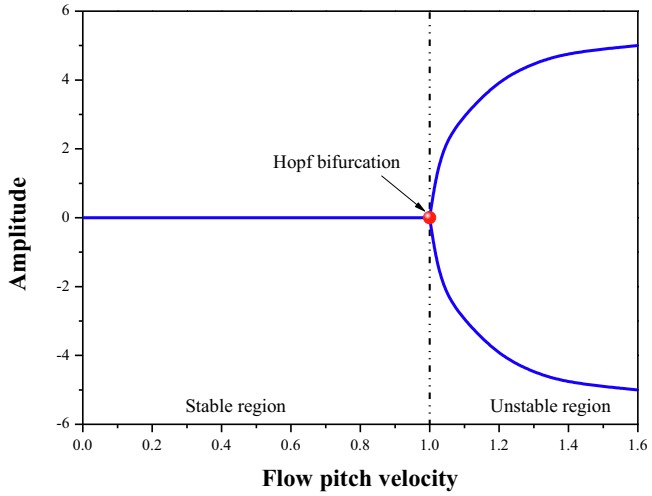

Fig. 14. Schematic bifurcation diagram and the critical velocity of the fluidelastic instability.

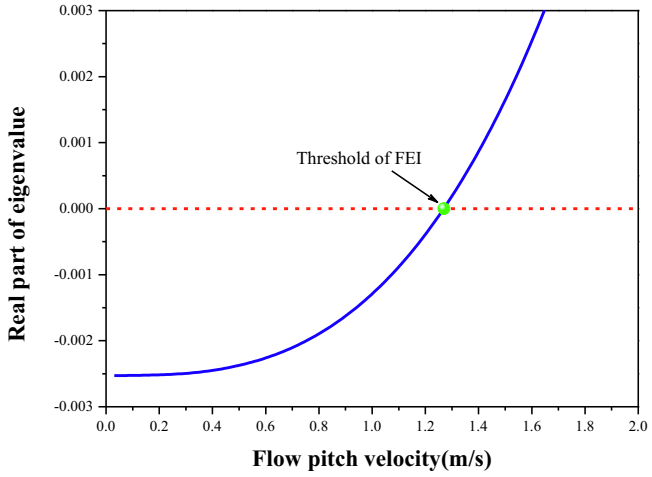

Fig. 15. The real part of the eigenvalues of the tube versus flow pitch velocity.

is important to note that the amplitude of the beat vibration is less than the gap between the tube bundles and support structures indicating that no collision occurs, the complex vibration behavior may affect the mechanical characteristics of the tube bundles. In other words, the beat vibration induced by the periodic force in the rotated triangular tube array is a typical forced vibration that is different from the vortex shedding vibration. And, the frequency of the periodic fluid force could have a significant influence on the vibration characteristics of the tube bundles before the fluidelastic instability. Besides, it is also important to note that, in varying tube array patterns, the frequency of the periodic fluid is different. Thus, the vibration analysis of the tube bundles considering the effect of the periodic fluid force should be performed to check out whether the resonance would happen during the steam generator design stage.

When the flow pitch velocity is larger than the threshold of the fluidelastic instability, the fluidelastic instability of the tube bundles occurs, causing an impact vibration between the tube bundles and the support structures. Fig. 17 shows the vibration responses and impact force of the central tube at U_p = 1.3 m/s. It can be seen that the impact vibration is a kind of multifrequency oscillation caused by a small disturbance. As shown in Fig. 17, once the vibration amplitude is larger than the gap between the tube and the support structures, the collision occurs, which could be the most important reason for early damage of the tube bundles. The effect of the impact vibration of the tube bundles on the fretting wear between the tube and support structure will be discussed in a future study.

5. Conclusions

Experimental and numerical studies were conducted to investigate the fluid–structure interaction of a rotated triangular tube array in cross-flow. In the experiment, the vibration responses of the tube bundles were measured. A mathematical model was presented to analyze the vibration characteristics of the tube bundles considering the effects of the periodic fluid force before the onset of fluidelastic instability. To obtain the frequency of the periodic fluid force acting on the rotated triangular tube array with

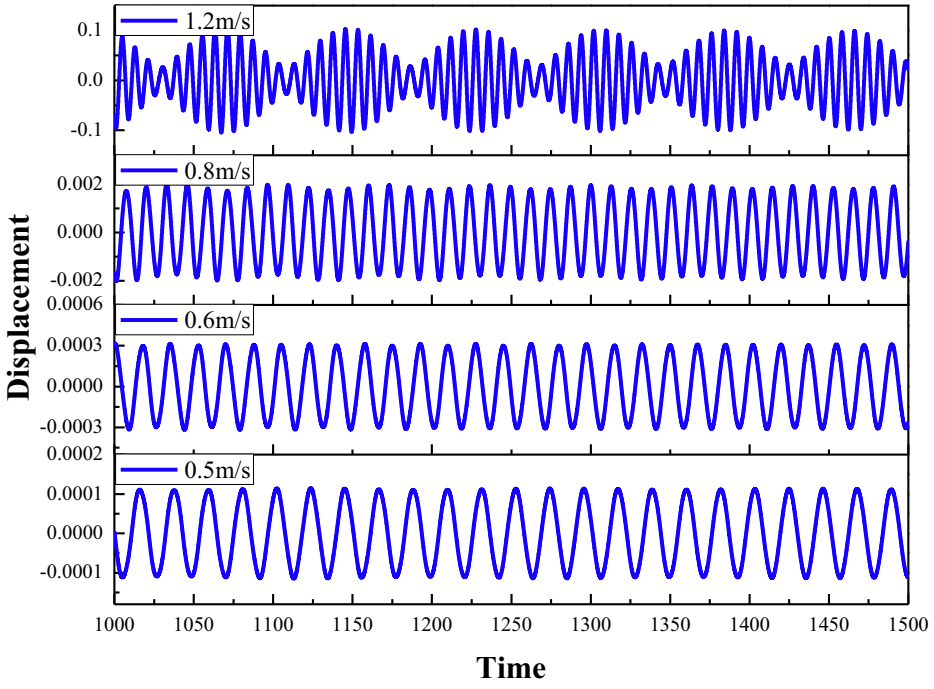

Fig. 16. Vibration response of the tube.

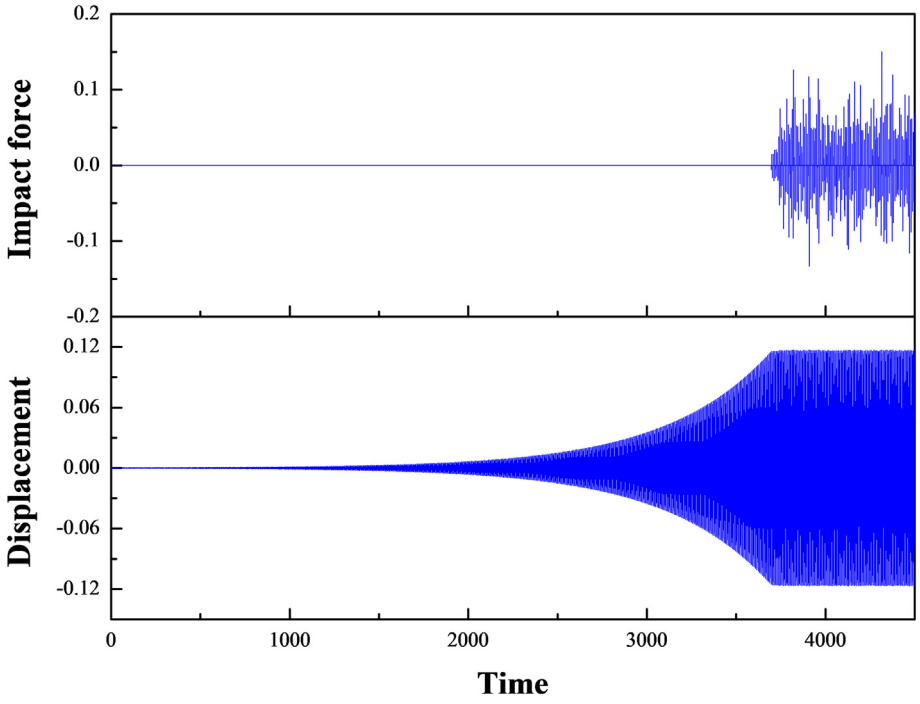

Fig. 17. The vibration response and impact force of the tube at U_p = 1.3 m/s.

P/D = 1.48, the Computational Fluid Dynamics was presented. Considering the effect of the periodic fluid force, the vibration responses of the tube bundles were calculated. From these analyses, we have drawn the following conclusions:

1. The critical velocity of a rotated triangular tube array with P/D = 1.48 subjected to cross-flow was obtained in the experiment. Before the fluidelastic instability, the beat vibration of the tube bundles occurs. The beat vibrations with large amplitude and multifrequency are different from the vibration characteristics of the fluidelastic instability
2. The transient analysis of the periodic fluid force in a rotate triangular tube array was conducted with the flow pitch velocity ranging from 0.5 m/s to 1.5 m/s. The numerical results show that the Strouhal number of the periodic fluid force in a rotated triangular tube array with P/D = 1.48 is about 0.42, and presents fewer variations when the flow pitch velocity ranging from 0.5 m/s to 1.5 m/s.
3. Considering the effect of the periodic fluid force and clearance restriction, the vibration responses of the tube bundles were calculated. It was found that the frequency of the periodic fluid force has a significant influence on the vibration characteristics of the tube bundles before the fluidelastic instability, which should be considered during the steam generator design stage.
4. When the flow pitch velocity is larger than the threshold of the fluidelastic instability, the fluidelastic instability of the tube bundles occurs, causing an impact vibration between the tube bundles and the support structures, which could be the most important reason for early damage of the tube bundles.

Declaration of Competing Interest

The authors declare that they have no known competing financial interests or personal relationships that could have appeared to influence the work reported in this paper.

Acknowledgment

This work was supported by the National Natural Science Foundation of China: [Grant Number 12072336].

References

Austermann, R., Popp, K., 1995. Stability behavior of a single flexible cylinder in rigid tube arrays of different geometry subjected to cross-flow. J. Fluids Struct. 9, 303–322.
Axisa, F., Antunes, J., Villard, B., 1990. Random excitation on heat exchanger tubes by cross-flow. J. Fluids Struct. 4, 321–341.
Borsoi, L., Piteau, P., Delaune, X., Antunes, J., 2017. Competition between turbulence and fluid-elastic forces in response of a loosely supported tube under cross-flow. Procedia Eng. 199, 1282–1289.
Chu, I.C., Chung, H.J., Lee, C.H., 2009. Fluid-elastic instability of rotated square array U-tubes in air-water flow. J. Pressure Vessel Technol. 131 (041301), 1–8.
Chung, H.J., Chu, I.C., 2006. Fluid-elastic instability of rotated square tube array in an air-water two-phase cross-flow. Nucl. Eng. Technol. 38 (1), 69–80.
Elhelaly, A., Hassan, M., Mohany, A., Moussa, S.E., 2020. Effect of the flow approach angle on the dynamics of loosely-supported tube arrays. Nucl. Eng. Des. 368, 110802.
Harran, G., 2014. Influence of the mass ratio on the fluidelastic instability of a flexible cylinder in a bundle of rigid tubes. J. Fluids Struct. 47, 71–85.
Hassan, M., Hayder, M., 2008. Modelling of fluidelastic vibrations of heat exchanger tubes with loose supports. Nucl. Eng. Des. 238, 2507–2520.
Hassan, M., Mohany, A., 2016. Simulation of fluidelastic forces and fretting wear in U-bend tube bundles of steam generators: Effect of tube-support conditions. Wind Struct. 23 (2), 157–169.
Janzen, V.P., Hagberg, E.G., Pettigrew, M.J., Taylor, C.E., 2005. Fluidelastic instability and work-rate measurements of steam-generator U-tubes in air-water cross-flow. J. Pressure Vessel Technol. 127, 84–91.
Lai, J., 2019. Analysis on streamwise fluidelastic instability of rotated triangular tube arrays subjected to two-phase flow. Mech. Syst. Sig. Process. 123, 192–205.
Lai, J., Sun, L., Gao, L., Tan, T., Xi, Z., Li, P., 2019. Study on fluidelastic instability of a tube array subjected to two-phase cross-flow. Ann. Nucl. Energy 126, 303–311.
Lai, J., Sun, L., Li, P., Tan, T., Gao, L., Xi, Z., He, C., Liu, H., 2019. Eigenvalue analysis on fluidelastic instability of a rotated triangular tube array considering the effects of two-phase flow. J. Sound Vib. 439, 194–207.
Lai, J., Sun, L., Li, P., 2019. Two-phase flow-induced instability and nonlinear dynamics of a single tube in tube bundles in the transverse direction. Eur. J. Mechan./A Solids 78, 103858.
Lai, J., He, C., Sun, L., Tan, T., 2020a. Theoretical and experimental study on the fluidelastic instability of tube bundles in two-phase cross flow. Int. J. Press. Vessels Pip. 181, 104069.

Lai, J., Sun, L., Gao, L., Li, P., Tan, T., 2020b. Theoretical investigation of fluidelastic instability of a rotated triangular tube array in two-phase flow. Arch. Appl. Mech. https://doi.org/10.1007/s00419-01725-z.
Lai, J., Wu, H., Sun, L., Gao, L., Li, P., 2020c. Numerical investigation on Hopf bifurcation and post-instability of tube bundles subjected to two-phase cross-flow and loose support. Ann. Nucl. Energy 143, 107459.
Lai, J., Sun, L., Gao, L., Tan, T., Li, P., 2020d. Two-phase flow-induced instability and nonlinear dynamics of a rotated triangular tube array in parallel direction. Eur. J. Mechan./A Solids 83, 104024.
Lai, J., Zhang, D., Sun, L., Gao, L., Tan, T., Li, P., 2020e. Investigation on fluidelastic instability of tube bundles considering the effect of slip ratio of air-water two-phase flow. Ann. Nucl. Energy 144, 107530.
Langre, E.D., Villard, B., 1998. An upper bound on random buffeting forces caused by two-phase flows across tubes. J. Fluids Struct. 12, 1005–1023.
Lever, J.H., Weaver, D.S., 1986b. On the stability of heat exchanger tube bundles. Part II: Numerical results and comparison with experiments. J. Sound Vib. 107 (3), 393–410.
Lever, J.H., Weaver, D.S., 1986a. On the stability of heat exchanger tube bundles. Part I: Modified theoretical model. J. Sound Vib. 107 (3), 375–392.
Nakamura, T., Fujita, K., Kawanishi, K., Yamaguchi, N., Tsuge, A., 1992. Study on the vibrational characteristics of a tube array caused by two-phase flow, part 2: fluidelastic vibration. J. Pressure Vessel Technol. 114, 479–485.
Paidoussis, M.P., Li, G.X., Rand, R.H., 1991. Chaotic motions of a constrained pipe conveying fluid: Comparison between simulation, analysis, and experiment. J. Appl. Mech. 58, 559–565.
M. P. Paidoussis. Flow induced vibration in nuclear reactors and heat exchangers: practical experiences and state of knowledge. IUTAM-IAHR Symposium on Practical Experiences with Flow Induced Vibrations (eds E. Naudascher and D. Rockwell), pp. 1-81. Berlin: Springer-Verlag.
Palomar, B.P., Meskell, C., 2018. Sensitivity of the damping controlled fluidelastic instability threshold to mass ratio, pitch ratio and Reynolds number in normal triangular arrays. Nucl. Eng. Des. 331, 32–40.
Pettigrew, M.J., Tromp, J.H., Taylor, C.E., 1989. Vibration of tube bundles in two-phase cross-flow. Part 2: Fluidelastic instability. J. Pressure Vessel Technol. 111, 478–487.
Price, S.J., Paidoussis, M.P., 1986. A constrained-mode analysis of the fluidelastic instability of a double row of flexible circular cylinders subject to cross-flow: A theoretical investigation of system parameters. J. Sound Vib. 105 (1), 121–142.
Sawadogo, T., Mureithi, N., 2014. Fluidelastic instability study in a rotated triangular tube array subject to two-phase cross-flow. Part I: Fluid force measurements and time delay extraction. J. Fluids Struct. 49, 1–15.
Shinde, V., Longatte, E., Baj, F., Braza, M., 2018. A theoretical model of fluidelasti instability in tube arrays. Nucl. Eng. Des. 337, 406–418.
Taylor, C.E., Currie, I.G., Pettigrew, M.J., Kim, B.S., 1989. Vibration of tube bundles in two-phase cross-flow Part 3: Turbulence-induced excitation. J. Pressure Vessel Technol. 111, 488–500.
Taylor, C.E., Pettigrew, M.J., 2000. Random excitation forces in heat exchanger tube bundles. J. Pressure Vessel Technol. 122, 509–514.

Further reading

Paidoussis, M.P., Semler, C., 1993. Nonlinear and chaotic oscillations of a constrained cantilevered pipe conveying fluid: A full nonlinear analysis. Nonlinear Dyn. 4, 655–670.